Synthesis and photoelectric property of poly(3-octylthiophene)/ferric oxide complexes

Zhiyue Han · Jingchang Zhang · Xiuying Yang · Hong Zhu · Weiliang Cao

Abstract Ferric oxide was prepared by the supercritical fluid drying (SCFD) method. A conducting polymer composite, poly(3-octylthiophene)/ferric oxide (POT/Fe_2O_3) was first synthesized through the chemical method. X-ray diffraction (XRD), X-ray Photoelectron Spectroscopy (XPS), and Infrared spectroscopy (IR) show that there is a chemical interaction in the composite, which indicates that Fe_2O_3 was successfully coated by poly(3-octylthiophene) molecules. The energy gap of the poly(3-octylthiophene)/ferric oxide composite is lower at 0.448 eV, which also shows that the optical performance of the new material is far superior to POT or Fe_2O_3 separately, by Ultraviolet–Visible spectra (UV–Vis) and fluorescence spectroscopy (PL). Solar cell was sensitized by POT/Fe_2O_3. A solar-to-electric energy conversion efficiency of 0.258% was attained with the system.

Introduction

Conducting polymers with highly extended π-electron systems in their main chains have attracted a great deal of interest [1]. Nanocomposites formed from oxide particles and intrinsically conducting polymers have repeatedly been described in the literature [2–6]. The original performance of the nanocomposite was improved because of the introduction of inorganic compound. The composite materials have better performance characteristics than the single component alone and even show improved functional features due to the effects of nanotechnology and the synergies between polythiophene and inorganic compound.

Recently, some articles have reported about such type of composite materials. N. Hebestreit et al. [7] has described about a composite of polythiophene (PT) and nano-titanium dioxide (TiO_2), which was synthesized via oxidative polymerization of thiophene using $FeCl_3$. The electrochemical measurements showed the nature of the p–n junction. G.D.Sharma [8] investigated the charge transport and photocurrent generation in poly(phenyl-azomethane-thiophene)/zinc oxide (PPAT:ZnO) bulk. It is found that the device with 55 wt% of ZnO in the blend shows maximum value of power conversion. Solar cells based on polymer materials [9–16] and ferric oxide [17–23] could in principle offer the advantage of production in high volume at low process cost. Research on the subject has focused mainly on improving the power conversion efficiency for small laboratory cells [24–26] through optimization of materials and the protocol used for preparation.

The supercritical fluid drying (SCFD) method was first reported by Kistier [27] in 1931, through which we can extract the dispersive phase from gel without destroying the frame structure because of the special characteristics of supercritical fluid. The problem of particle agglomeration during the drying process was solved effectively. This method can be used to prepare solids with high surface area, high pore volume, low density, low refractive index, and low thermal conductivity. The SCFD method is also considered as an effective way to yield the nanosized materials and is, therefore, widely used [28–30].

There are many studies in the literature on solar cells based on the hybrid of poly(3-hexylthiophene) (P3HT) and

Z. Han · J. Zhang (✉) · H. Zhu · W. Cao
Institute of Modern Catalysis, Beijing University of Chemical Technology, State Key Laboratory of Chemical Resource Engineering, Beijing 100029, China
e-mail: zhangjc1@mail.buct.edu.cn

J. Zhang · X. Yang · W. Cao
Hainan Institute of Science and Technology, Haikou 571126, China

other material [31–37]. However, there are very few with regard to poly(3-octylthiophene) and ferric oxide nano-composites.

The process of preparing the ferric oxide by the SCFD method is described in detail in this article. poly(3-octyl-thiophene) and nano-scale Fe_2O_3 particles were combined to form a new organic/inorganic composite material through chemical reaction. The chemical interaction in the material was confirmed during the analyses using Infrared Spectrum, X-ray Diffraction, and X-ray Photoelectron Spectroscopy. Results from UV–Vis spectra and Fluorescence spectra indicate that POT/Fe_2O_3 nanocomposite is a kind of promising material with excellent performance characteristics in photoelectric applications. It has also been found that the initial oxidation/reduction potential of nanocomposite is lower than individual components, which demonstrates that the conductivity of nanocomposite is higher than individual components.

Experimental details

Synthesis of poly(3-octylthiophene)/ferric oxide nanocomposite

Preparation of nano-Fe_2O_3 by supercritical fluid drying method

Surfactant AEO-3 (0.3v %) was added to 0.3 mol/L $Fe(NO_3)_3$, stirring vigorously at ambient temperature. The pH of the solution was adjusted to be 8–9 through dropwise addition of ammonia. After aging for 16 h, the sol was filtered and washed until no presence of NO_3^- was confirmed. The water in the sol was replaced by absolute ethanol. The alcogel was then transferred into the high-pressure autoclave, with the addition of ethanol as a supercritical fluid. The quantity of ethanol added was three-fifths of the volume of autoclave. The solution was then sealed and heated at increased pressure—to ensure that the pressure of liquid is greater than the vapor pressure during the whole process—with a heating rate of 100 °C/h. Ethanol is maintained in the supercritical state for 30 min at 243 °C, the fluid is then released, and purged with nitrogen to remove residual ethanol and water, followed by natural cooling to room temperature. The powders of ferric oxide aerogels were thus finally obtained.

Synthesis of poly(3-octylthiophene)

Synthesis of poly(3-octylthiophene) with Fe(III) as catalyst is performed as described earlier [38]. Thiophene with alkyl side chain length ($n = 8$) was used for the polymer synthesis. A solution comprising 20 mL chloroform and 0.03 mol anhydrous $FeCl_3$ was taken in a 100-mL flask with the import and export of nitrogen as liquid droplets, and kept under stirring for about 15 min. A solution of 0.01 mol monomer dissolved in 20 mL chloroform was then gradually added dropwise to the solution in the flask, until the latter becomes a dark green turbid liquid. The temperature of system was controlled. After the completion of the above process, the system was reacted at room temperature with high-purity nitrogen as shielding gas for 7 h. The resulting product was slowly added to 300 mL methanol which was followed by a settlement and filtration. The residual black solid was added to 50 mL chloroform in a conical flask, accompanied by stirring for 60 min and a gentle heating. As a result, a sanguine chloroform solution was obtained. After distilling the chloroform solution, small amounts of viscous liquid residue were added to 200 mL methanol and slowly allowed to settle. The precipitates were dried in vacuum at room temperature; subsequently, they were washed by methanol in a soxhlet extraction for 20 h and further distilled by chloroform. After settlement in 200 mL methanol and vacuum drying at room temperature, the pure polymer was obtained.

Synthesis of poly(3-octylthiophene)/ferric oxide nano-composite

Some chloroform, 3-octylthiophene, and Fe_2O_3 prepared as described in "Preparation of nano-Fe_2O_3 by supercritical fluid drying method" were taken in a flask, and ultrasonic dispersing was performed for about 15 min. Some $FeCl_3$ was dissolved in chloroform, and then gradually poured dropwise into the flask. Then, the system was allowed to react under stirring and high-purity nitrogen gas shielding for 7 h. The resulting product was slowly added into methanol, followed by a settlement and filtration. Then, the precipitates were washed in methanol in a soxhlet extraction unit for 20 h. POT/Fe_2O_3 nanocomposite powder was finally obtained by vacuum drying at room temperature.

After dissolving 0.01 g POT/Fe_2O_3 in 2 mL isopropyl alcohol, the resulting solution is spread out evenly on a clean quartz glass and ITO conductive glass. Then, red-brown POT/Fe_2O_3 nanocomposite films were obtained by means of vacuum drying method.

Solar cell sensitized by POT/Fe_2O_3

Nanocrystalline TiO_2 films coated with a monolayer of POT/Fe_2O_3 were incorporated in a thin-layer regenerative solar cell equipped with a light-reflecting counter electrode.

Measurements

X-ray diffraction (XRD) measurements were performed using a Shimadzu HR6000X (Cu target X tube, voltage 40.0 kV, current 30.0 mA). Infrared spectra (IR) were recorded using a prestige-21IR spectrophotometer with KBr pellet. X-ray Photoelectron Spectroscopy (XPS) analyses were conducted by ESCALAB 250, testing the electronic binding energy of the samples. UV–Vis spectra were measured using Hitachi U-3010 spectrophotometer. The Fluorescence spectra were measured using Hitachi F-7000 spectrofluorophotometer at room temperature. Cyclic voltammetry measurements were carried out with the Potentiostiostat/Galvanostat (EG&G PAR Model 283). The counterelectrode used was platinum and the reference electrode was non-aqueous Ag/Ag^+. The CV curves were recorded in acetonitrile with 0.1 M $LiClO_4$ at a scan rate of 50 mV/S. Before using, the solution was insufflated with N_2 for 30 min. Current–voltage (I–V) measurements were taken in air at room temperature (298 K) using a Keithley 236 high current source power meter under white-light illumination from a 500 W Xenon lamp. The light intensity was about 50mW/cm^2 on the sample surfaces measured by a photodetector. In order to measure the decay, the short circuit current (I_{SC}), and open circuit voltage (V_{OC}) as a function of the illumination time were recorded.

Results and discussion

TEM measurements of Fe_2O_3

Figure 1 demonstrated TEM results of nano-Fe_2O_3 prepared by SCFD method. As seen from the electron microscope photographs, the powder particles prepared by SCFD method are found to be of uniform size and dispersed well, with a size range of 15–20 nm. The results are basically in accordance with the Scherrer formula. Han et al. [39] demonstrated that the average particle size of
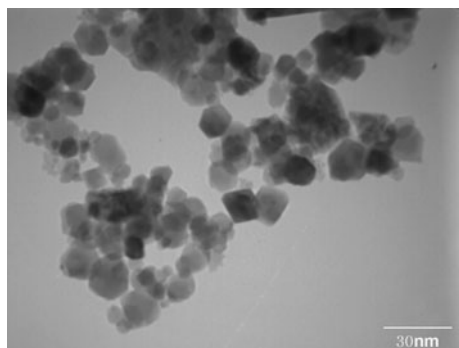

Fig. 1 TEM patterns of Fe_2O_3

nano-oxide prepared by SCFD method is the smallest, and that the SCFD method can perform both dryness and crystallization in one single step. Therefore, the SCFD was chosen as the preferred method for the preparation of the nanosized Fe_2O_3.

XRD characterization of POT/Fe_2O_3

The XRD patterns for the POT, Fe_2O_3, and POT/Fe_2O_3 nanocomposites are shown in Fig. 2. For the POT, the "hill" at 15–28° is connected to amorphous phase, while the reflections at around 5.52°, 9.56°, 13.96°, and 24.76° can reflect crystalline structure. Reflection at 24.76° is attributed to interchain distance between π-stacking oxidized chains. Bragg equation gives 0.31 nm for this value. Reflections at 5.52°, 9.56°, and 13.96° Bragg angles prove the layered structure of POT, having a dominant first-order reflection at $2\theta = 5.52°$ indicating the lamellar interlayer spacing as 1.60 nm [23]. The diffraction peak of POT is quite narrow, which shows its high degree of crystallization, plane structure, and the highly consistent, orderly manner of POT segment. It can be seen from XRD patterns of Fe_2O_3 particles that the peaks at $2\theta = 24.16°$, 33.28°, 35.74°, 40.99°, 49.50°, 54.23°, 57.56°, 62.26°, 64.18°, 69.58°, 72.03°, 75.37,° and 77.55° are assigned to the (012), (104), (110), (113), (024), (116), (122), (214), (300), (208), (1 0 10), (217), and (306) lattice planes of the hexagonal crystalline α-Fe_2O_3, respectively. The average Fe_2O_3 particle is calcuated as 19 nm by Scherrer formula. The results are basically in accordance with the TEM measurements. For the POT/Fe_2O_3 composites, the XRD data mainly show the strong Fe_2O_3 peaks. The characteristic POT broad peak cannot be seen easily on the XRD patterns of POT/Fe_2O_3 composite. The XRD patterns of the
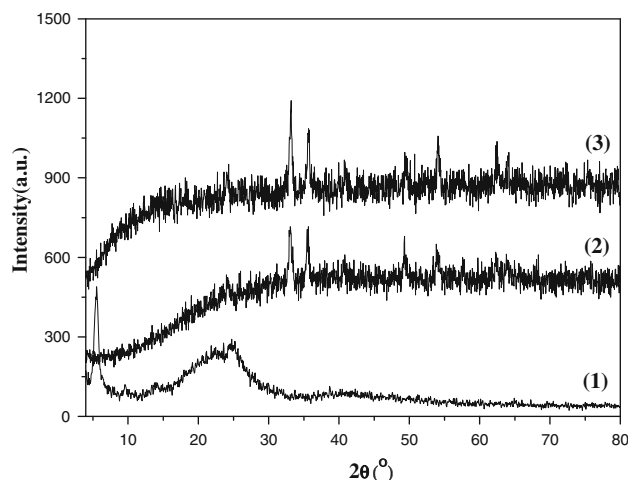
**Fig. 2** XRD patterns of (1) POT, (2) POT/Fe_2O_3, and (3) Fe_2O_3 nanocomposite

nanocomposites have higher background intensity, lower diffraction peak intensities, decreased interplaner spacing, and reduced sharpness of the peak profiles than pure Fe_2O_3, which confirmed the chemical interaction between POT and nano-Fe_2O_3.

XPS characterization of POT/Fe_2O_3

Figure 3a–e shows the high-resolution XPS spectra of sample POT, Fe_2O_3, and POT/Fe_2O_3. The XPS binding energy of the Fe 2p in sample Fe_2O_3 is consistent with the data found in referrence [40]. It was seen that Fe in Fe_2O_3 mainly existed in trivalence. Figure 3a shows the narrow scans for Fe 2p peaks located at 710.28 eV (Fe $2p_{3/2}$) and 723.93 eV (Fe $2p_{1/2}$) of the POT/Fe_2O_3. The results confirm that compared with Fe_2O_3, lower binding energy shift took place obviously. This indicates that Fe atom must have interacted with some atom other than O after

composite reaction. Two sulfur peaks (S2p3/2) were found: one with the binding energy of 164 eV corresponding to neutral thiophene units in the polymer chain, and the other with the binding energy of 165 eV corresponding to oxidized thiophene units (see the separate graphics in Fig. 3b, c), within the enlarged binding energy scale between 160 and 170 eV [41, 42]. In the investigated examples, 34.12% of the peak areas lies at 165 eV in POT and 22.31% of the peak area in POT/Fe_2O_3. This indicates that S atom will interact with some atom other than C after composite reaction. In Fig. 3e, two oxygen peaks at 530.80 and 528.75 eV are found in the XPS spectra of Fe_2O_3, one corresponding to oxygen in crystal lattice, and the other corredsponding to oxygen adsorbed on the surface of Fe_2O_3. Four oxygen peaks at 533.65, 532.50, 530.80, and 528.75 eV are found in the XPS spectra of POT/Fe_2O_3, 532.50 eV for POT, 530.80 and 528.75 eV for Fe_2O_3 (see the separate graphics in Fig. 3d–f). A strong peak at

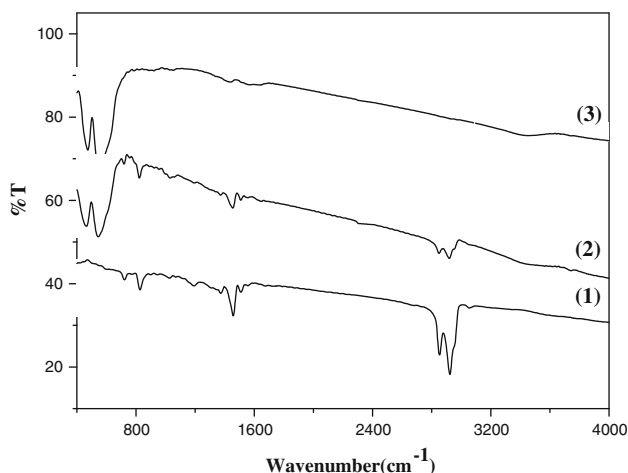**Fig. 3** XPS spectra of POT, Fe_2O_3, and POT/Fe_2O_3 nanocomposite
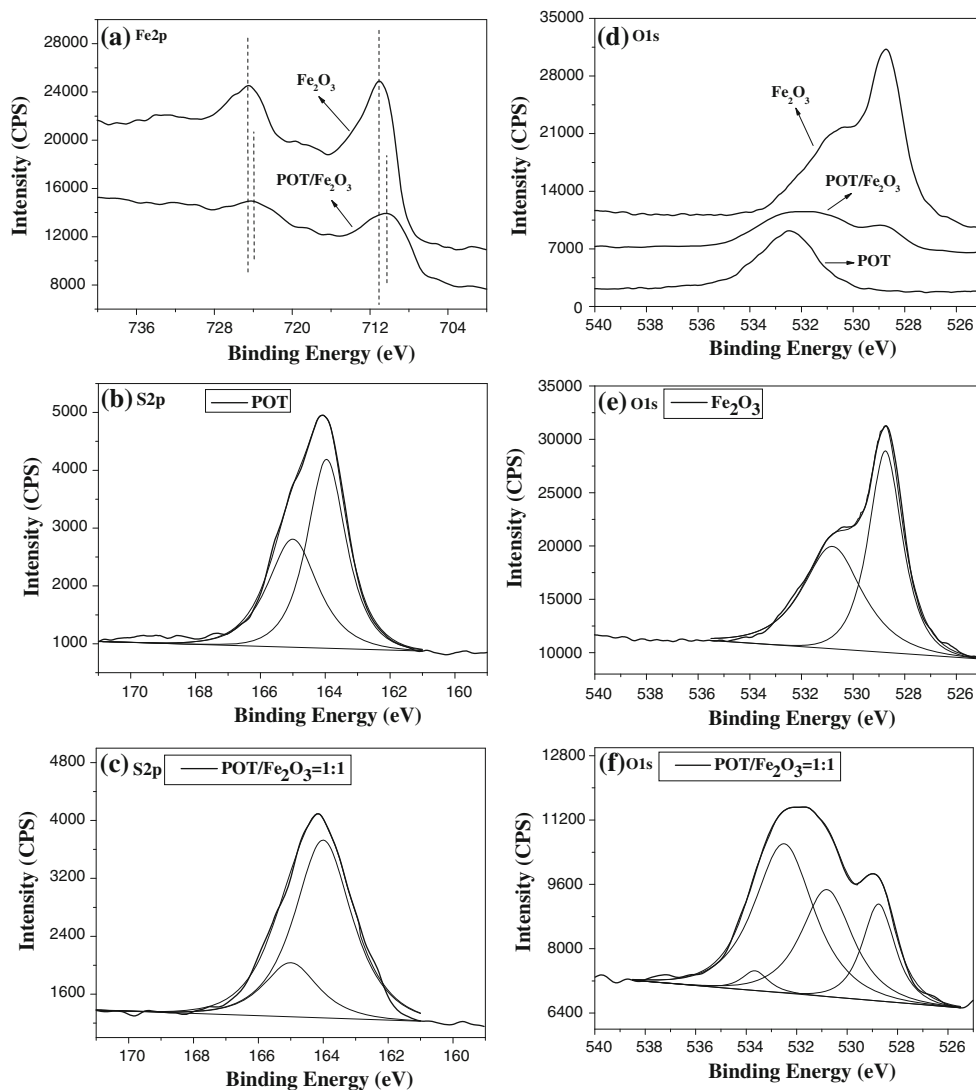
533.65 eV was obtained when fitting the oxygen peak curve. It indicates that O atom will interact with some atom other than C and Fe after composite reaction. It is inferred that there are two kinds of the chemical interaction: one between the π-stacking chains of POT and the O in the surface of Fe_2O_3, and the other between the S of POT and the Fe in the surface of Fe_2O_3.

IR spectra results of POT/Fe_2O_3

Figure 4 shows the FT-IR spectra of POT, Fe_2O_3, and POT/Fe_2O_3 nanocomposite. In the spectrum of POT, a low-intensity peak can be visualized at 3052 cm^{-1}, which can be attributed to the thiophene ring C–H stretching vibration, one at 1190 cm^{-1} which can be due to the C_α–C_α single resonance absorption, and one at 828 cm^{-1} due to C–H$_\beta$ out-of-plane bending of a 2,3,5-trisubstituted thienylene moiety. It indicates that there is a predominant α–α coupling of thiophenes on polymerization. The C–H of CH_2 or CH_3 symmetric and asymmetric stretching at 2926 and 2849 cm^{-1} correspond to asymmetric and symmetric deformations at 1370 cm^{-1}; the bands at 1513 and 1465 cm^{-1} correspond to thiophene ring C=C stretching vibrations of symmetric and asymmetric, respectively; The bands at 718 cm^{-1} correspond to methylenes vibration [43]. These results suggest that the poly 3-octyl thiophene was synthesized successfully.

The characteristic absorption bands of Fe–O–Fe at about 472 and 565 cm^{-1} can be seen in the FT-IR spectrum of the Fe_2O_3 particles, which correspond to Fe–O stretching and bending vibrations, respectively, and these two broad bands become sharper and narrower in the POT/Fe_2O_3. Bands coming from both Fe_2O_3 and POT were observed in the spectrum of POT/Fe_2O_3 nanocomposite, whereas the

Fig. 4 FT-IR spectra of (1) POT, (2) POT/Fe_2O_3, and (3) Fe_2O_3 nanocomposite
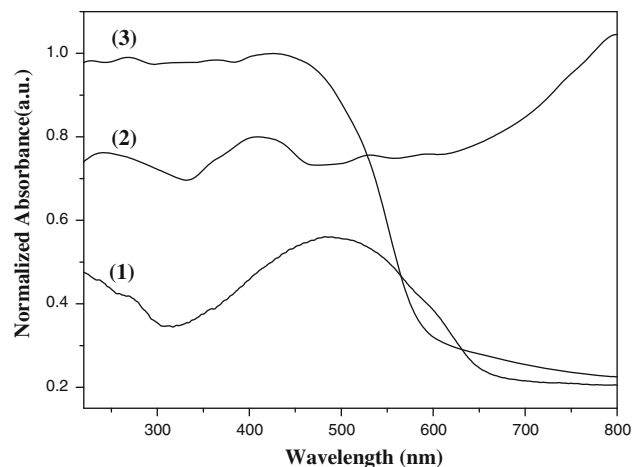
Fig. 5 UV–Visible absorption spectra of (1) POT, (2) POT/Fe_2O_3, and (3) Fe_2O_3 nanocomposite

bands originating from Fe_2O_3 and POT were located at low wavenumber. This again confirmed the chemical interaction taking place between POT and nanosized Fe_2O_3.

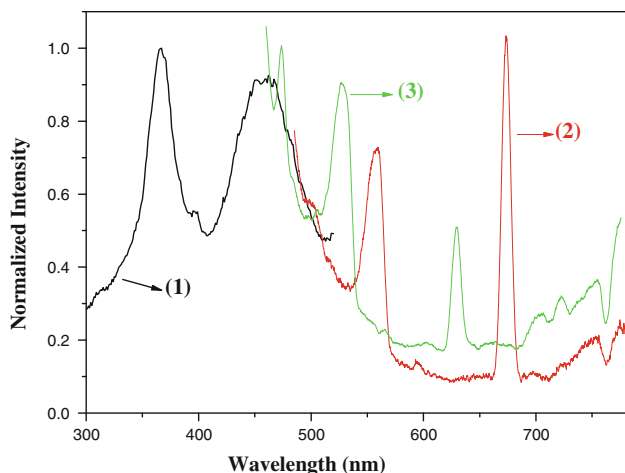UV–Vis spectra of POT/Fe_2O_3 nanocomposite film

The UV–Vis spectra of the POT solid film, Fe_2O_3, and POT/Fe_2O_3 nanocomposite films are presented in Fig. 5. As expected, Fe_2O_3 shows the characteristic spectrum with its fundamental absorption of Fe–O bond into UV light region ranging from 220 nm to 550 nm. The UV–Vis spectrum of POT indicates that POT has maximum adsorption at a wavelength of about 489 nm for the π–π^* transition. From the spectrum of POT/Fe_2O_3 nanocomposite film, it can be seen that there were three absorption bands with maximum wavelengths of 242, 409, and 531 nm in UV region and visible light region respectively. The band ranging from 220 to 330 nm was assigned to the characteristic absorption bands of Fe_2O_3 and the POT in the UV light region. The other two bands were attributed to the electron transition from the valence bond to the antibonding polaron state (π–π^* type) of POT. [44, 45] Compared with the spectrums of Fe_2O_3 and POT, the POT/Fe_2O_3 nanocomposite film absorbs much more UV–Vis light, obviously. It is reasonable to believe that POT/Fe_2O_3 nanocomposite may perform better in semiconductor than POT and Fe_2O_3.

Fluorescence spectra of POT/Fe_2O_3 nanocomposite film

The fluorescence spectra of the POT solid film, Fe_2O_3, and POT/Fe_2O_3 nanocomposite films are shown in Fig. 6. The emission peak of POT ranging from 300 to 500 nm can be

Fig. 6 Fluorescence emission spectra of (*1*) POT, (*2*) POT/Fe$_2$O$_3$, and (*3*) Fe$_2$O$_3$ nanocomposite

seen in Fig. 6, with the maximum emission at 367 and 463 nm. There also were three emission peaks in the fluorescence spectra of Fe$_2$O$_3$, and the maximum emission wavelengths were 473, 527, and 630 nm. The fluorescence spectrum of POT/Fe$_2$O$_3$ nanocomposite flim was totally different from either POT or Fe$_2$O$_3$. There are two main bands in visible light region, with their λex values being about 557 and 674 nm, respectively. It exhibited improved optical property for the new chemical interaction between POT and Fe$_2$O$_3$. These results once again proved that POT/Fe$_2$O$_3$ is a new improved compound.
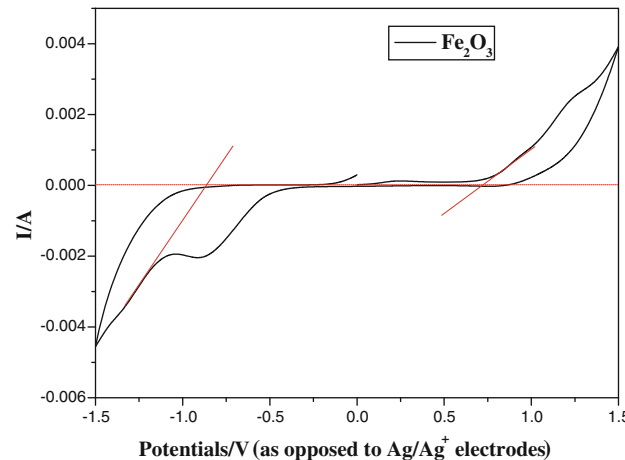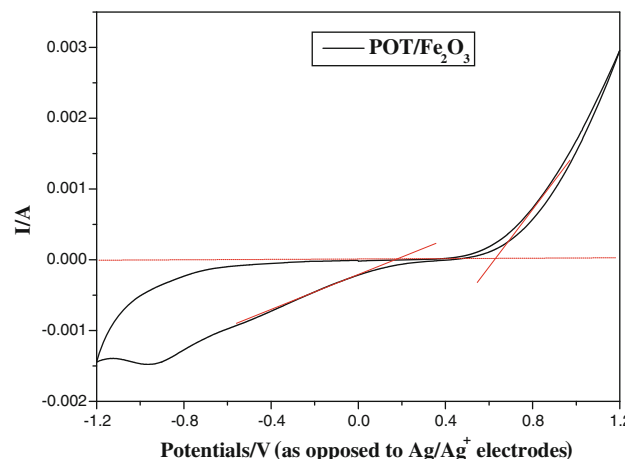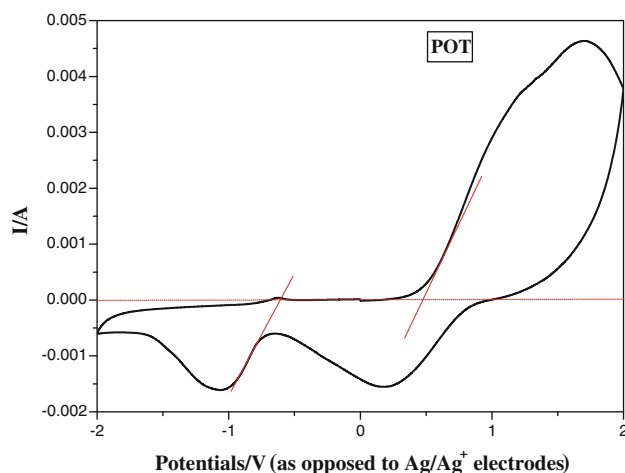
Cyclic voltammetry

The frontline molecular orbital and energy gap of POT, Fe$_2$O$_3$, and POT/Fe$_2$O$_3$ nanocomposites are listed in Table 1. Figure 7 shows that oxidation area of POT was larger than reduction area, and that the initial oxidation potential was fairly low. The characteristics above indicated that POT was a *p*-type semiconductor. Fe$_2$O$_3$ was an *n*-type semiconductor. It can be seen from the cyclic

Table 1 the frontline molecular orbital and energy gap of POT, Fe$_2$O$_3$, and POT/Fe$_2$O$_3$

Sample	Φox (eV)	Φred (eV)	EHOMO (eV)	ELUMO (eV)	Eg (eV)
POT	0.470	−0.610	−4.910	−3.830	1.080
POT:Fe$_2$O$_3$ = 1:1	0.633	0.185	−5.073	−4.255	0.448
Fe$_2$O$_3$	0.731	−0.866	−5.171	−3.574	1.597

Φox and Φred potentials (versus 0.01 Ag$^+$/Ag in CH$_3$CN) determined by cyclic voltammetry. Calculated according to Eg = Φox − Φred. EHOMO and ELUMO from EHOMO = −(Φox + 4.44) eV, and ELUMO = −(Φred + 4.44) eV
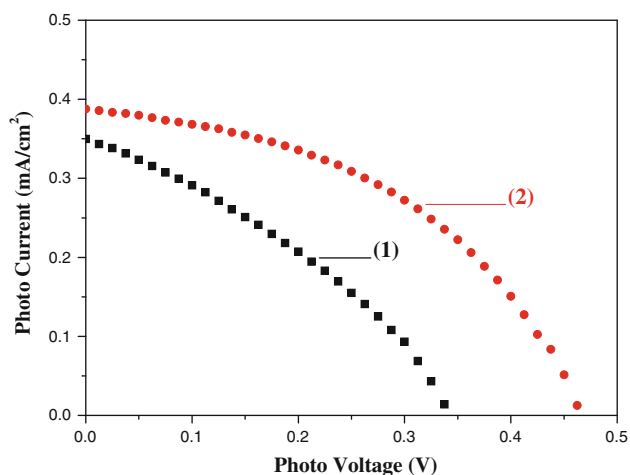

Fig. 7 Cyclic voltammetry curves of POT, Fe$_2$O$_3$, and POT/Fe$_2$O$_3$ nanocomposite

voltammogram curves of POT/Fe$_2$O$_3$ nanocomposites films that initial oxidation potential of POT/Fe$_2$O$_3$ nanocomposite films was obliviously lower than each single component while initial reduction potential was higher. The

energy gap of POT/Fe$_2$O$_3$ nanocomposite is only 0.448 eV. The results indicated that POT/Fe$_2$O$_3$ composite could be a new promising p–n type composite material.

Performance parameters of dye-sensitized solar cells

The performance characteristics of the photovoltaic device are shown in Fig. 8 and all the parameters of POT- and POT/Fe$_2$O$_3$-sensitized solar cell are listed in Table 2. Under standard global AM 1.5 (50 mW/cm^2) solar condition, the POT-sensitized solar cell gives a short circuit voltage short-circuit current (Jsc) of 0.350 mA/cm^2, open-circuit voltage (Voc) of 0.350 V, effective area of 0.963 cm^2, and fill factor (FF) of 0.338, corresponding to an overall conversion efficiency (η) of 0.086%; the POT/Fe$_2$O$_3$-sensitized solar cell gives a short circuit voltage short-circuit current (Jsc) of 0.387 mA/cm^2, open-circuit voltage (Voc) of 0.475 V, effective area of 0.660 cm^2, and fill factor (FF) of 0.444, corresponding to an overall conversion efficiency (η) of 0.258%. The overall conversion efficiency enhancement of POT/Fe$_2$O$_3$ relative to POT can be attributed to the chemical interaction in the composite, as described in "XPS characterization of POT/Fe$_2$O$_3$". In the UV–Vis spectra, the POT/Fe$_2$O$_3$ nanocomposite films absorb much more visible light, and so the incident photon-to-current conversion efficiency was high.

Conclusions

Ferric oxide was prepared by the supercritical fluid drying (SCFD) method. A conducting polymer composite, poly (3-octylthiophene)/ferric oxide (POT/Fe$_2$O$_3$) was first synthesized through the chemical reaction. X-ray diffraction (XRD), X-ray Photoelectron Spectroscopy (XPS, and Infrared spectroscopy (IR) analyses show that chemical interaction takes place in the composite, indicating that Fe$_2$O$_3$ was successfully coated by poly(3-octylthiophene) molecules. The energy gap of the POT/Fe$_2$O$_3$ composite is decreased to 0.448 eV, which also shows that the optical performance of the composite material is far superior to POT or Fe$_2$O$_3$ when used alone, as confirmed by Ultraviolet–Visible (UV–Vis) spectra and fluorescence spectroscopy (PL). Solar cell was sensitized by POT/Fe$_2$O$_3$. A solar-to-electric energy conversion efficiency of 0.258% was attained with the improved material. The results show that POT/Fe$_2$O$_3$ nanocomposites are promising materials with excellent performance characteristics in photoelectric applications.

Fig. 8 Photochemical study of POT and POT/Fe$_2$O$_3$ nanocomposite

Table 2 Performance parameters of dye-sensitized solar cells

Dye	Jsc (mA/cm^2)	Voc (V)	ff	η (%)
POT	0.350	0.350	0.338	0.086
POT:Fe$_2$O$_3$ = 1:1	0.387	0.475	0.444	0.258

References

1. McCullough RD (1998) Adv Mater 10:93
2. Gangopadhyay R, De A (2000) Chem Mater 12:608
3. Gomez-Romero P (2001) Adv Mater 13:163
4. Malinauskas A (2001) Polymer 42:3957
5. Caruso F (2001) Adv Mater 13:11
6. Hill PG, Foot PJS, Davis R (1996) Synth Met 76:289
7. Hebestreit N, Hofmann J, Rammelt U, Plieth W (2003) Electrochim Acta 48:1779
8. Sharma GD (2008) Synth Metal 158:400
9. Brabec CJ, Sariciftci NS, Hummelen JC (2001) Adv Funct Mater 11:15
10. Spanggaard H, Krebs FC (2004) Sol Energy Mater Sol Cells 83:125
11. Coakley KM, McGehee MD (2004) Chem Mater 16:4533
12. Hoppe H, Sariciftci NS (2004) J Mater Res 19:1924
13. Winder C, Sariciftci NS (2004) J Mater Chem 14:1077
14. Bundgaard E, Krebs FC (2007) Sol Energy Mater Sol Cells 91:954
15. Günes S, Neugebauer H, Sariciftci NS (2007) Chem Rev 107:1324
16. Jorgensen M, Norrman K, Krebs FC (2008) Sol Energy Mater Sol Cells 92:686
17. Aroutiounian VM, Arakelyan VM, Shahnazaryan GE, Stepanyan GM, Turner John A, Khaselev O (2002) Int J Hydr Energy 27:33
18. Halmann M, Zuckerman K (1988) Solar Energy Mater 17:311
19. Chia-Lin T, Chung-Jen T, Jyh-Chen C (2010) Int J Hydr Energy 35:2781
20. Maheshwar S, Prasad BM (1983) Solar Energy Mater 8:457

21. Smestad G, Ennaoui A, Fiechter S, Tributsch H, Hofmann WK, Birkholz M, Kautek W (1990) Solar Energy Mater 20:149
22. Arico AS, Antonucci V, Giordano N, Crea F, Antonucci PL (1991) Mater Chem Phys 28:75
23. Visy C, Bencsik G, Nemeth Z, Vertes A (2008) Electrochim Acta 53:3942
24. Li G, Shrotriya V, Huang J, Yao Y, Moriarty T, Emery K, Yang Y (2005) Nat Mater 4:864
25. Ma W, Yang C, Gong X, Lee K, Heeger AJ (2005) Adv Funct Mater 15:1617
26. Kim JY, Lee K, Coates NE, Moses D, Nguyen TQ, Dante M, Heeger AJ (2007) Science 317:222
27. Kisstler SS (1931) Nature 127:741
28. Zhang J, Li Q, Cao W (2003) Chin J Catal 24:831
29. Zhang J, Gao L, Cao W (2006) J Rare Earths 24:182
30. Wan Y, Ma J, Zhou W (2004) Appl Catal A Gen 277:55
31. Bouclé J, Chyla S (2008) Comptes Rendus Physique 9:110
32. Park S, Tark SJ, Lee JS, Lim H, Kim D (2009) Sol Energy Mater Sol Cells 93:1020
33. Wang M, Wang X (2008) Sol Energy Mater Sol Cells 92:766
34. Kim H, So WW, Moon SJ (2007) Sol Energy Mater Sol Cells 91:581
35. Motaung DE, Malgas GF, Arendse CJ, Mavundla SE, Oliphant CJ, Knoesen D (2009) Sol Energy Mater Sol Cells 93:1674
36. Zimmermann B, Wurfel U, Niggemann M (2009) Sol Energy Mater Sol Cells 93:491
37. Wang M, Wang X (2007) Sol Energy Mater Sol Cells 91:1782
38. Sugimoto R (1986) Chem Express 1:635
39. Han Z, Zhang J, Yang X, Zhu H, Cao W. doi:10.1007/s10854-009-9956-6
40. Wagner CD, Riggs WM, Davis LE et al (1976) X-ray photo electron spectroscopy. Perkin Elmer, Eden Prairie, MN, p 76
41. Kang ET (1992) Macromolecules 25:6842
42. Kang ET (1991) Phys Rev B 44:10461
43. Karim MR, Lee CJ, Lee MS (2006) J Polym Sci A: Polym Chem 44:5283
44. Mark JE (1999) Polymer data handbook. Oxford University Press, Oxford
45. Patil AO, Heeger AJ, Wudl F (1988) Chem Rev 88:183